



JGR Space Physics

RESEARCH ARTICLE

10.1029/2020JA028182

Key Points:

- The recently released Gravity field and steady-state Ocean Circulation Explorer (GOCE) cross-track wind data have been compared with winds measured by ground-based FPIs at low and middle latitudes
- During geomagnetically quiet periods, GOCE crosswinds are 1.37–1.69 times larger than the ground-based FPIs winds
- The GOCE crosswinds agree better with the ground-based FPIs winds at geomagnetically quiet periods than those at active periods

Supporting Information:

Supporting Information may be found in the online version of this article.

Correspondence to:

G. Jiang, gyjiang@spaceweather.ac.cn

Citation:

Jiang, G., Xiong, C., Stolle, C., Xu, J., Yuan, W., Makela, J. J., et al. (2021). Comparison of thermospheric winds measured by GOCE and ground-based FPIs at low and middle latitudes. *Journal of Geophysical Research: Space Physics*, 126, e2020JA028182. https:// doi.org/10.1029/2020JA028182

Received 30 APR 2020 Accepted 21 DEC 2020

Comparison of Thermospheric Winds Measured by GOCE and Ground-Based FPIs at Low and Middle Latitudes

Guoying Jiang^{1,2,3}, Chao Xiong², Claudia Stolle², Jiyao Xu^{1,3}, Wei Yuan^{1,3}, Jonathan J. Makela⁴, Brian J. Harding⁵, Robert B. Kerr⁶, Günther March^{7,8}, and Christian Siemes⁸

¹National Space Science Center, State Key Laboratory of Space Weather, Chinese Academy of Sciences, Beijing, China, ²GFZ German Research Centre for Geosciences, Potsdam, Germany, ³School of Astronomy and Space Science, University of Chinese Academy of Sciences, Beijing, China, ⁴Department of Electrical and Computer Engineering, University of Illinois at Urbana-Champaign, Urbana, IL, USA, ⁵Space Sciences Laboratory, University of California, Berkeley, USA, ⁶Scientific Solutions Inc, Chelmsford, MA, USA, ⁷Department of Astrodynamics and Space Missions, Faculty of Aerospace Engineering, Delft University of Technology, HS Delft, the Netherlands, ⁸RHEA for ESA - European Space Agency, Noordwijk, the Netherlands

Abstract The re-estimates of thermospheric winds from the Gravity field and steady-state Ocean Circulation Explorer (GOCE) accelerometer measurements were released in April 2019. In this study, we compared the new-released GOCE crosswind (cross-track wind) data with the horizontal winds measured by four Fabry-Perot interferometers (FPIs) located at low and middle latitudes. Our results show that during magnetically quiet periods the GOCE crosswind on the dusk side has typical seasonal variations with largest speed around December and the lowest speed around June, which is consistent with the ground-FPI measurements. The correlation coefficients between the four stations and GOCE crosswind data all reach around 0.6. However, the magnitude of the GOCE crosswind is somehow larger than the FPIs wind, with average ratios between 1.37 and 1.69. During geomagnetically active periods, the GOCE and FPI derived winds have a lower agreement, with average ratios of 0.85 for the Asian station (XL) and about 2.15 for the other three American stations (PAR, Arecibo and CAR). The discrepancies of absolute wind values from the GOCE accelerometer and ground-based FPIs should be mainly due to the different measurement principles of the two techniques. Our results also suggested that the wind measurements from the XL FPI located at the Asian sector has the same quality with the FPIs at the American sector, although with lower time resolution.

1. Introduction

Thermospheric wind is an important participant in the electro-dynamic and hydro-dynamic processes of upper atmosphere. The characteristics of thermospheric wind is thus a necessary and effective tool for understanding the coupling of Earth's thermosphere-ionosphere system. For decades, scientists have been trying to extend our knowledge about thermospheric wind, which in the upper thermosphere has been measured by several techniques, including: (1) remote sensing with optical instruments, for example, Fabry-Perot interferometers (FPIs) (Biondi & Feibelman, 1968; Burnside & Tepley, 1989; Emmert et al., 2001; Killeen et al., 1982; Noto et al., 1994; Rees et al., 1980; Shepherd et al., 1993; Wu et al., 2004, 2008); (2) ground-based incoherent scatter radar measurements (Balsley et al., 1976; Emery, 1978; Lei et al., 2007); (3) the detections of satellite drag, for example, accelerometers (King-Hele, 1964; King-Hele & Walker, 1983; Marcos & Forbes, 1985; Lühr, et al., 2007; T. Visser et al., 2019); and (4) in situ observations with neutral mass spectrometer (Spencer et al., 1981). Short introductions for each technique have been provided in Lühr et al. (2007) and references therein. In addition to the observations, another important tool for interpreting the upper atmospheric wind dynamics is numerical modeling. Several observed properties of neutral wind can be reproduced rather well, for example by the Horizontal Wind Model (HWM) (Drob et al., 2015; Hedin et al., 1988) and the National Center for Atmospheric Research's Thermosphere, Ionosphere and Electrodynamics General Circulation Model (NCAR TIEGCM) (Richmond et al., 1992).

A method of wind derivation from electrostatic tri-axial accelerometer instruments mounted on several spacecraft in the early 1980s was described by Marcos and Forbes (1985). The acceleration experienced by

© 2020. American Geophysical Union. All Rights Reserved.

JIANG ET AL. 1 of 16

a LEO satellite below about 500 km is mainly due to atmospheric drag. By assuming proper values of the drag coefficient and attitude-dependent effective cross sectional area of the satellite in the ram direction, thermospheric density and wind (mainly the cross-track component, in the following named "crosswind") can be derived. In recent years, the accelerometers from the Challenging Minisatellite Payload (CHAMP) and Gravity field and steady-state Ocean Circulation Explorer (GOCE) missions provided excellent opportunities to estimate thermospheric winds (Doornbos et al., 2010; Doornbos, 2011; Liu et al., 2006; March et al., 2019a, 2019b; Sutton, 2008; Visser & van den IJssel, 2016; Visser et al. 2018; T. Visser et al., 2019). The continuous wind measurements during their mission period significantly extended our knowledge of wind dynamics in the upper atmosphere, in perspectives of global, seasonal, local time, as well as solar and geomagnetic activity responses (M. Dhadly et al. 2017; M. S. Dhadly et al. 2018; Doornbos et al., 2014; Liu et al., 2006, 2016; Lühr et al., 2007; Xiong et al., 2015; Zhang et al., 2017). In addition, the GOCE crosswind data have been included in the HWM14 model for improving the wind predictions at geomagnetic quiet periods (Drob et al., 2015).

GOCE was launched on March 17, 2009 and reentered the Earth's atmosphere on November 11, 2013. Comparisons between GOCE derived winds (different from the version used in this study) with other observations and models have been reported earlier. Kärräng (2015) compared GOCE crosswinds with the ground-based horizontal wind observations from Scanning Doppler Imagers (SDIs) and FPIs located in the northern hemisphere: Poker Flat, Alaska (65.12°N, 32.57°W), HAARP, Alaska (62.39°N, 34.86°W), Toolik, Alaska (68.63°N, 30.4°W), Kiruna, Sweden (67.53°N, 21.04°E) and Longyearbyen, Svalbard (78.15°N, 16.04°E). The GOCE crosswinds and the ground-based sounded winds show moderate to good correlations with correlation coefficients from 0.60 to 0.89. The absolute values of GOCE wind vectors were found to be 1.2–2.0 times larger than the ground-based measurements (as the slope of linear regression indicated). Liu et al. (2016) found that the HWM14 model shows consistent seasonal variations with GOCE zonal wind data, but the wind speed is somehow lower than the GOCE measurement by values of \sim 20 m/s. M. Dhadly et al. (2017) and M. S. Dhadly et al. (2019) compared the GOCE crosswind with winds derived from the WIND Imaging Interferometer (WINDII) on the Upper Atmosphere Research Satellite (UARS), and ground-based SDI and FPI located at Poker Flat and Toolik Lake, Alaska. They found that the GOCE measured wind generally correlates well with the other observations on the dawn side, but relatively larger discrepancies are found on the dusk side. Aruliah et al. (2019) compared high-latitude thermospheric winds measured by two ground-based FPIs and CHAMP accelerometer, finding that the phases of the winds agree very well but CHAMP wind values at high latitudes are typically 1.5-2 times larger than FPI winds.

Recently, the GOCE accelerometer data have been recalibrated by improving the gas-surface interaction model (March et al., 2019b), and the new version (V2.0) of GOCE wind data have been released as part of the official ESA documentation (https://earth.esa.int/eogateway/missions/goce/goce+-thermospheric-data) on April 5, 2019. Therefore, in this study we perform a statistical comparison between the recalibrated GOCE wind data from 2010 to 2013 with ground-based measurements from FPIs located on the Asian and American sectors, ranging from around equatorial region to middle latitude. Both Kärräng (2015) and M. Dhadly et al. (2017) only compared the GOCE wind with FPI/SDI winds at high latitudes, so our work here adds by the comparison between low and middle latitudes FPI data and GOCE data.

The FPI is an optical system which measures the spectra of the emission lines from airglow or aurora. Wind and temperature can be estimated by analyzing the Doppler shift and the line width of these emissions, respectively (Biondi & Feibelman, 1968; Burnside & Tepley, 1989; Emery, 1978; Emmert et al., 2006a, 2006b; Innis & Dyson, 1996; Ishii et al., 1997; Kerr et al., 1989; Makela et al., 2012; Meriwether, 2006; Noto et al., 1994; Wu et al., 2004; Yu et al., 2014; Yuan et al., 2010).

Our comparison focuses on the dusk side during which there is better overlap than on the dawn side between the GOCE and FPI measurements. In addition, we want to offer a comprehensive empirical validation for the wind measurement of XL FPI in addition to the previous validation against model predictions in Jiang et al. (2018). The study is structured as follows: Section 2 describes the wind measurements from GOCE and various ground-based FPIs. Section 3 introduces the methods of data analysis. Section 4 presents the comparison results during both geomagnetic quiet (Kp < 3) and disturbed periods (Kp \ge 3). A discussion comparing the results with those from previous studies are given in Section 5. The final summary is presented in Section 6.

JIANG ET AL. 2 of 16

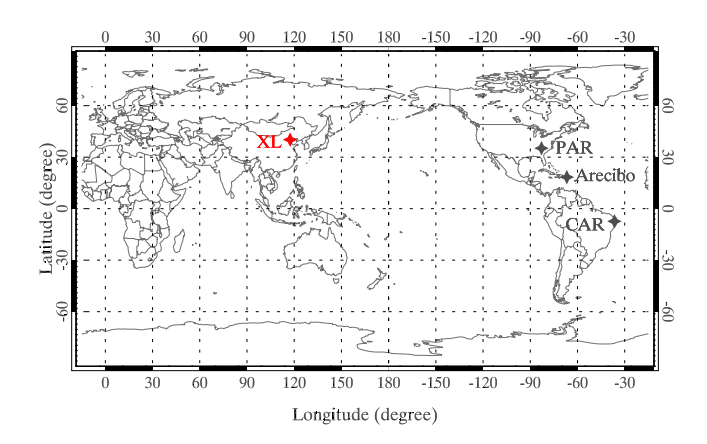


Figure 1. The location distribution of four ground-based FPI systems used in our study. FPI, Fabry-Perot interferometers; GOCE, Gravity field and steady-state Ocean Circulation Explorer.

2. Wind Measurements and Methods of Data Analysis

2.1. GOCE Satellite and Crosswind

The GOCE satellite was launched into a Sun-synchronous dusk-dawn orbit with an inclination of 96.7°. Its mission period starts on March 17, 2009 and ends on November 11, 2013, which spans from low to increased solar activity. The primary objective of GOCE was to precisely measure the static part of Earth's gravity field and ocean circulation (Floberghagen et al., 2011). Fortunately, the on-board accelerometers provide an excelent opportunity to derive thermospheric mass density and crosswinds. For details about the updated processing algorithm of recalibrated GOCE wind data, readers are referred to March et al. (2019b). The crosswind component at low and middle latitudes is mainly in the zonal direction (Liu et al., 2016). GOCE wind data products include zonal, meridional and vertical components, which are computed by treating the crosswind as a vector. The in-track wind component from GOCE cannot be measured due to the large drag contribution. A comprehensive description of the wind retrieval and the data set is provided in March et al. (2019b).

In this study, GOCE crosswinds of version 2.0 data set are employed to do comparison with the winds observed by ground FPIs. The time span of GOCE data used in our comparison is from 2010 to 2013, and the satellite altitude decreased from about 260 to 220 km during this period.

2.2. FPI Observations

In this study, we use measurements from four FPIs located in Asian and American longitude sectors, and their locations are shown in Figure 1 and detailed in Table 1.

The XL FPI is located at Xinglong Observatory (geog.: 40.2°N, 117.4°E; geom.: 35°N), China. XL FPI belongs to the Chinese Meridian Project (Wang, 2010), and its routine observation started in April 2010. This FPI was designed to have three filter channels for measuring the OH 892.0 nm (~87 km), OI 557.7 nm (~97 km) and OI 630.0 nm (~250 km) nightglow emissions. There are five directions sampled in each sequence, including the zenith direction and four cardinal directions (east, west, north, and south) with 45° elevation angle. The integration time is 3 min for OH 892.0 nm and OI 557.7 nm, and 5 min for OI 630.0 nm. Time resolution (or duty cycle) for each wind field (both meridional and zonal components) is about 1 h. The detail of the XL FPI, its operation and the wind data processing method, can be found in Wu et al. (2004) and Yuan et al. (2010, 2013). Jiang et al. (2018) reported that XL FPI has the reliable local time, seasonal, and longitudinal variations of thermospheric horizontal winds at mid-latitudes during geomagnetically quiet times by comparing with winds from an empirical wind model and a numerical model. The red line (630.0 nm) wind data from April 2010 to November 2013 are employed in the GOCE-FPI wind comparison presented in this study.

The PAR FPI was installed at the Pisgah Astronomical Research Institute (geog.: 35.2°N, 82.85°W; geom.: 45.8°N), USA, in June 2011, which is one site of the North American Thermosphere Ionosphere Observation

Table 1 Data Sets of Ground-Based FPIs Used in This Paper				
Station	Geographic location	Geomagnetic latitude	Years of data	Detection wavelength (nm)/Height (km)
XL	40.2°N, 117.4°E	35°N	April 2010–November 2013	630.0/250
PAR	35.2°N, 82.85°W	45.8°N	June 2011–November 2013	630.0/250
Arecibo	18.35°N, 66.75°W	27.1°N	May 2012-November 2013	630.0/250
CAR	7.38°S, 36.52°W	11.74°S	July 2010–November 2013	630.0/250

JIANG ET AL. 3 of 16

Network (NATION) (Makela et al., 2012). Thermospheric wind and temperature can be obtained using the observation of the spectral line shape of the 630.0 nm redline emission from O_2^+ dissociative recombination at ~250 km. There are two measurement modes in PAR FPI operation: cardinal mode and common volume mode (Fisher, 2013; Fisher et al., 2015). Cardinal mode is the standard data collection process including four line of sight measurements in directions of north, east, south and west at a 45° elevation angle followed by a zenith exposure. Common volume mode is a more complicated coordinated observation, which was described in Makela et al. (2013). The details of measurement and wind data processing of PAR FPI can be found in Fisher (2013, 2017), Harding (2017), Harding et al., (2017a, 2017b). In this study, the wind data calculated from the cardinal mode are chosen for the GOCE-FPI wind comparison. The data time span used is from June 2011 to November 2013.

The CAR FPI was installed in Cariri (geog.: 7.38°S, 36.52°W; geom.: 11.74°S), Brazil in 2009. This FPI is part of the Remote Equatorial Nighttime Observatory for Ionospheric Regions (RENOIR) network (Fisher, 2013; Harding, 2017; Makela et al., 2009). The thermospheric wind and temperature from the 630.0 nm redline emissions were collected from the measurements of cardinal mode and common volume mode. In cardinal mode, the CAR FPI operated independently and simply cycled through the four cardinal directions (north, east, south and west at a 45° elevation angle) and the local zenith (Makela et al., 2013). The details of measurement and wind data processing of CAR FPI can be found in Makela et al. (2011), Fisher (2013, 2017), Harding (2017), Harding et al., (2017a, 2017b). In this study, the wind data observed by cardinal mode are chosen for GOCE-FPI wind comparison. Data time span is from July 2010 to November 2013.

A new redline FPI system at Arecibo Observatory (geog.: 18.35° N, 66.75° W; geom.: 27.1° N) began to monitor the thermospheric 630.0 nm emission of OI at ~ 250 km altitude since May 2012 (Kerr, 2013, 2019; Kerr et al., 2017). The standard operating mode is to record measurements in four cardinal directions (North, South, East, and West) at a 45° elevation angle, with a fifth measurement in the zenith. For each direction, the exposure time is 4 min. Kerr (2013) described the system operating and data processing of Arecibo FPI in details. The wind data of cardinal mode measurements from May 2012 to November 2013 are used in this work.

2.3. Methods of Data Analysis

For the XL FPI, data measured in nice weather during moon phase <85% are selected. In addition, wind estimates with uncertainty greater than 40 m/s are not considered, and winds with absolute speed greater than 300 m/s are also omitted. For the PAR and CAR FPIs, we kept the observations in good weather and moon phase <85%. The estimated wind data with fit uncertainty greater than 25 m/s or with absolute speed greater than 300 m/s are discarded. In addition, these two instruments provide quality flags. Measurements associated with quality flags (WIND_ERR) of 2, equating to "bad quality" are also discarded. The information of cloud measurements for PAR and CAR are included in the WIND_ERR flag, so cloud coverage is actually taken into account. For Arecibo, we kept the observations in good weather, during moon phase <85%, and with quality flag = 0, 1. Data with wind estimates having absolute speed greater than 300 m/s are not included. For GOCE observations, the measurements made during thruster inactive periods are excluded, as are data possibly affected by outliers, missing data, filter initialization effects, or eclipse transition.

We took three steps to find conjunction events between GOCE and each FPI station. First, only the orbits when the GOCE and FPI longitudinal difference was less than 15° have been considered. Second, for each selected orbit, the GOCE wind measurement within $\pm 5^{\circ}$ latitude centered on the FPI station are averaged as a new GOCE database, whose position is the measuring moment and location of orbit point closest to FPI latitude. Finally, the FPI winds measured within ± 0.5 hour around the new GOCE database are averaged to a new FPI database. In this way, we derived 134, 153, 196, and 233 conjunction events for XL, PAR, Arecibo and CAR stations, respectively.

Figure 2 presents the paired wind databases distribution as a function of date and universal time. Blue open circles and red solid stars denote the FPI winds and GOCE winds, respectively. Dusk side and dawn side are indicated at right side of each panel. Clearly seen here is that conjunction events are mainly found for the dusk side and rarely appear at dawn side. Therefore, we will focus only on the wind comparison on the dusk side in this study.

JIANG ET AL. 4 of 16

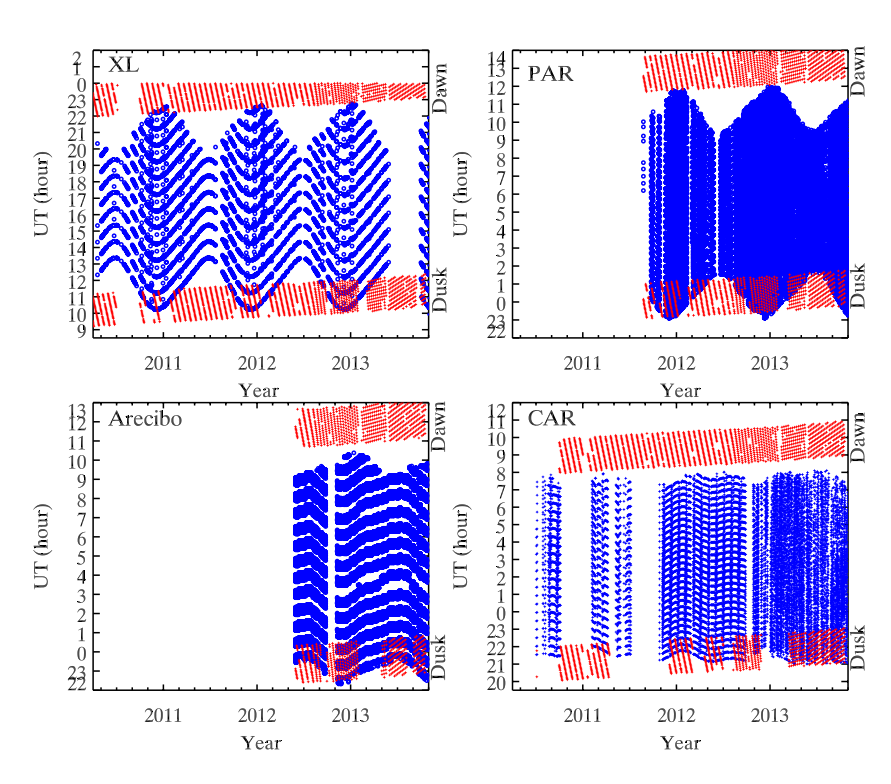


Figure 2. The paired wind databases distribution with year and universal time. Blue open circles and red solid stars denote FPI projected winds and GOCE crosswinds, respectively. Dusk side and dawn side are indicated at right side of each panel. FPI, Fabry-Perot interferometers; GOCE, Gravity field and steady-state Ocean Circulation Explorer.

The coincident winds of GOCE and FPIs are sorted separately into geomagnetic quiet (Kp < 3) and disturbed (Kp_{current} \geq 3 or Kp_{3 hours ago} \geq 3 or both) periods.

2.4. Wind Vector Projection

As Doornbos et al. (2013) mentioned, GOCE crosswinds represent the cross-track part of the winds, not the full vector zonal or meridional winds. Hence, to make the most reliable comparison between GOCE crosswinds and FPI winds, it is necessary to project the FPI horizontal winds (zonal and meridional components) onto the GOCE cross-track direction. Equation 1 outlines the applied method for wind vector projection:

$$a' = \vec{a} \cdot \hat{b} \tag{1}$$

Here, \vec{a} is the FPI horizontal wind vector; \hat{b} is the unit vector of GOCE crosswind, and $\hat{b} = \vec{b} / |\vec{b}|$; a' is the projected FPI wind vector in the GOCE crosswind direction. FPI projected winds are used for the statistical comparison. For all four stations, we first project the FPI winds to the GOCE cross-track direction and then compare with the GOCE crosswind.

3. Observations

3.1. During Geomagnetically Quiet Periods

Figure 3 shows the scatter-plot comparison of GOCE crosswinds and FPI projected winds at four stations during quiet periods. The first column presents the comparison during all seasons, and green lines give the linear fitting results between them. Patterns in the second to fourth columns present the results for different seasons. Here, the errors in the FPI data are assumed to be zero.

As indicated by the correlation coefficients (C_C) in Figure 3, the correlations between GOCE crosswinds and FPI projected winds are all around 0.6: 0.58 for XL, 0.67 for PAR, 0.68 for Arecibo and 0.64 for CAR. In different seasons or months, there are some differences in wind speeds at the four FPI stations. For

JIANG ET AL. 5 of 16

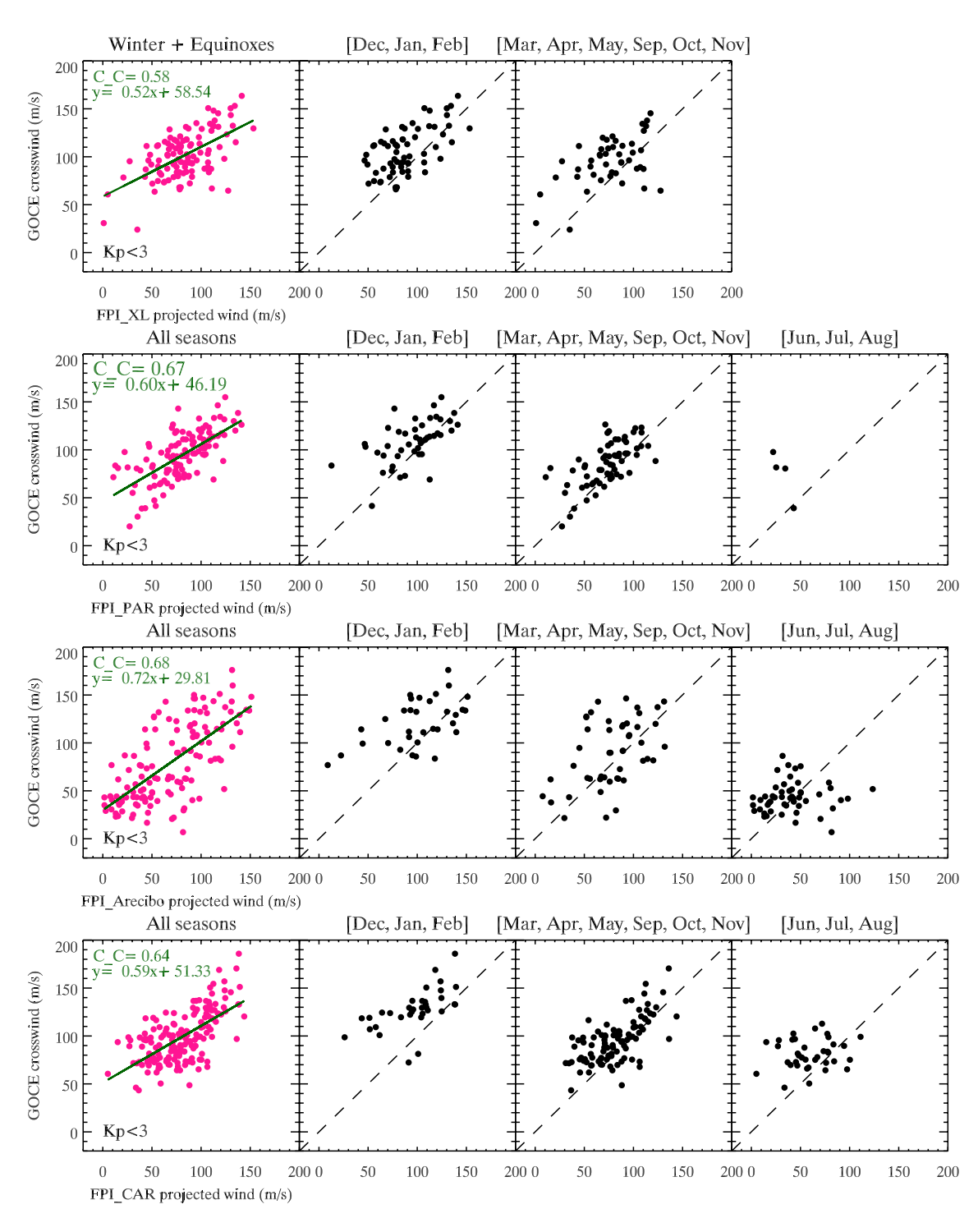


Figure 3. Scatterplot comparison of GOCE crosswinds and FPI projected winds during geomagnetically quiet time. The first column presents the wind comparison of the whole database collected from GOCE and FPIs. The second to fourth columns present the results of different seasons (local winter, equinoxes, and local summer). Green lines give the linear regression fit result of the observations from two systems; here, the errors in the FPI data are assumed to be zero. FPI, Fabry-Perot interferometers; GOCE, Gravity field and steady-state Ocean Circulation Explorer.

stations at middle latitude, GOCE crosswind speeds are basically larger than those of XL and PAR FPIs in all seasons; for low latitude station, GOCE and Arecibo FPI have relatively comparable wind speeds in the months of equinoxes, but GOCE crosswind shows larger speed than FPI wind in the months of December-January-February and June-July-August; for the station in equatorial region, GOCE crosswind shows

JIANG ET AL. 6 of 16

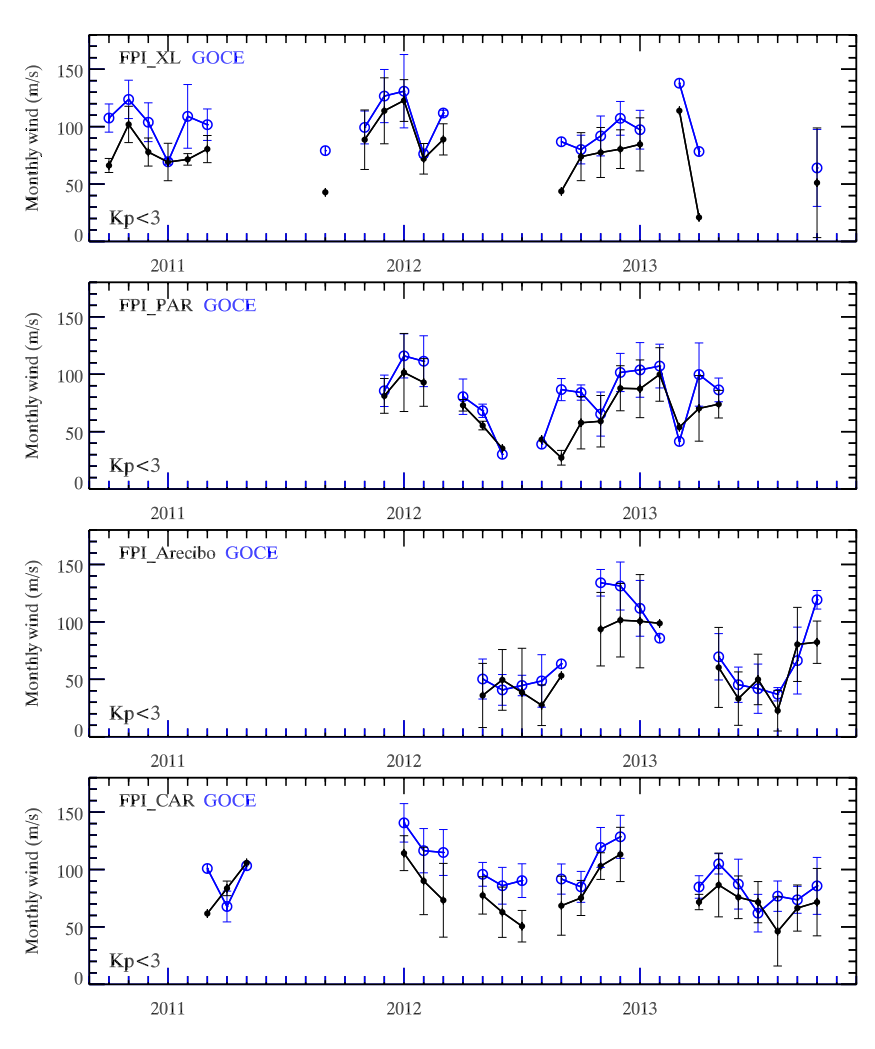


Figure 4. The monthly averaged values of conjunct winds on the dusk side from GOCE and FPIs during 2010–2013. The error bars are the variance in the data used in the monthly data. FPI, Fabry-Perot interferometers; GOCE, Gravity field and steady-state Ocean Circulation Explorer.

significantly larger speed than CAR FPI in all seasons. The intercepts of linear regression equation can give the bias information between two measurement systems (shown by the first column of Figure 3). During geomagnetically quiet periods, Arecibo FPI shows smaller bias (29.81 m/s) than other FPIs (58.54 m/s for XL, 46.19 m/s for PAR, 51.33 m/s for CAR) when comparing the FPI data in the crosswind direction.

The linear regression result with FPI data errors considered is given in the supplement of this paper. When considering the errors in the FPI data during, we found that during quiet times the slope increased by up to 21.67% for PAR, 15.28% for Arecibo and 37.29% for CAR, and the intercepts decreased by up to 22.28% or 10.29 m/s for PAR, 54.06% or 10.46 m/s for Arecibo and 63.78% or 19.99 m/s for CAR; During geomagnetically active times, the slope increased by up to 84.44% for PAR, 34.48% for Arecibo and 32.61% for CAR, and the intercepts decreased by up to 44.22% or 20.19 m/s for PAR, 8.7% or 3.85 m/s for Arecibo and 24.20% or 12.94 m/s for CAR. Correlation coefficients of the error-considered case and the zero-error case are comparable during quiet times.

The monthly averaged values of conjunction winds on the dusk side from GOCE and FPIs are illustrated in Figure 4, and the error bars are the variance of the data used in the monthly average. We can see that at low and middle latitudes, GOCE crosswinds are generally larger than FPI projected winds in most of the months from September 2010 to October 2013, but the winds from two systems have similar variations with time. At around 250 km altitude, GOCE crosswinds and FPI projected winds on the dusk side both show

JIANG ET AL. 7 of 16

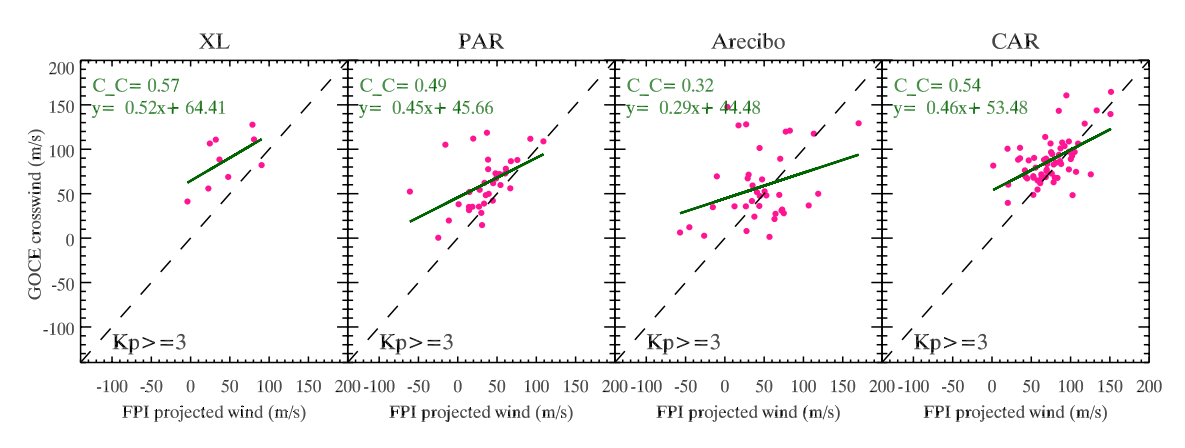


Figure 5. Scatterplot comparison of GOCE crosswinds and FPI projected winds during geomagnetically active periods. the green lines give the line fit result of the observations from two systems and the dashed lines are diagonal lines. FPI, Fabry-Perot interferometers; GOCE, Gravity field and steady-state Ocean Circulation Explorer.

a significant annual variation with the largest speed around December and the lowest speed around June from around equatorial region to middle latitude.

3.2. During Geomagnetically Active Periods

Figure 5 presents the scatter-plot comparison of GOCE crosswinds and FPI projected winds collected during geomagnetically active periods with $Kp_{current} \geq 3$ or $Kp_{3 \, hours \, ago} \geq 3$ or both. The green lines give the linear fitting of observations from two systems and the dashed lines are diagonal lines. Compared with the quiet periods, the correlations between them are smaller, with worst case for Arecibo. The values of C_C between GOCE and FPI winds are 0.57 for XL, 0.49 for PAR, 0.32 for Arecibo and 0.54 for CAR, respectively. GOCE wind measurements from middle latitude to around equatorial region (XL, PAR, and CAR) are generally larger than FPI observations. The intercepts of linear regression equation indicate the bias 44.48 m/s for Arecibo FPI, 64.41 m/s for XL FPI, 45.66 m/s for PAR FPI, 53.48 m/s for CAR FPI during the geomagnetically active periods.

Figure 6 presents the time series of GOCE crosswinds and FPI projected winds (same data groups as those in Figure 5) and their differences. The conjunction events found between GOCE and XL FPI are concentrated in months of equinox and boreal winter, and most events show larger wind speeds in the GOCE observation. A similar situation appears in the comparison of GOCE and PAR station: the crosswind derived from the accelerometer are generally larger than FPI projected winds during geomagnetically active periods in all seasons. At CAR (around equatorial region), GOCE crosswinds are generally larger than CAR FPI winds in most events. However, a different feature is found for the station at Arecibo, that GOCE crosswinds somehow have smaller speeds than FPI in boreal summer months especially in the summer of 2013, but have stronger winds in the months of January, September and October.

In addition to ordinary linear regression, another method incorporating the FPI data error into the linear regression has also been performed, and the results are given in the supplement of this study. During active times, correlation coefficients increased by up to 59.18% for PAR and 18.52% for CAR, but were similar for Arecibo.

3.3. Seasonal Variation Indicated by the Horizontal Winds of GOCE and FPI Measurements

Since GOCE flew on a near-polar sun-synchronous orbit, the crosswind direction is near to the zonal direction at low and middle latitudes (Doornbos et al., 2013). In order to confirm and show readers what this means, we present the zonal wind variations measured by GOCE and FPIs.

Figure 7 gives the time series of GOCE and FPIs zonal wind observations on the dusk side during geomagnetically quiet periods over the four stations, as well as the solar flux index $F_{10.7}$ during the years of 2010–2013. Here, the GOCE zonal winds are shown as gray crosses when it passes over the stations, regardless

JIANG ET AL. 8 of 16

21699402, 2021, 2, Downloaded from https://agupubs.onlinelibrary.wiley.com/doi/10.1029/2020IA028182, Wiley Online Library on [27/06/2024]. See the Terms and Conditions (https://onlinelibrary.wiley.com/doi/10.1029/2020IA028182, Wiley Online Library on [27/06/2024]. See the Terms and Conditions (https://onlinelibrary.wiley.com/doi/10.1029/2020IA028182, Wiley Online Library on [27/06/2024]. See the Terms and Conditions (https://onlinelibrary.wiley.com/doi/10.1029/2020IA028182, Wiley Online Library on [27/06/2024]. See the Terms and Conditions (https://onlinelibrary.wiley.com/doi/10.1029/2020IA028182, Wiley Online Library on [27/06/2024]. See the Terms and Conditions (https://onlinelibrary.wiley.com/doi/10.1029/2020IA028182, Wiley Online Library on [27/06/2024]. See the Terms and Conditions (https://onlinelibrary.wiley.com/doi/10.1029/2020IA028182, Wiley Online Library on [27/06/2024]. See the Terms and Conditions (https://onlinelibrary.wiley.com/doi/10.1029/2020IA028182, Wiley Online Library on [27/06/2024]. See the Terms and Conditions (https://onlinelibrary.wiley.com/doi/10.1029/2020IA028182, Wiley Online Library on [27/06/2024]. See the Terms and Conditions (https://onlinelibrary.wiley.com/doi/10.1029/2020IA028182, Wiley Online Library on [27/06/2024]. See the Terms and Conditions (https://onlinelibrary.wiley.com/doi/10.1029/2020IA028182, Wiley Online Library on [27/06/2024]. See the Terms and Conditions (https://onlinelibrary.wiley.com/doi/10.1029/2020IA028182, Wiley Online Library on [27/06/2024]. See the Terms and Conditions (https://onlinelibrary.wiley.com/doi/10.1029/2020IA028182, Wiley Online Library on [27/06/2024]. See the Terms and Conditions (https://onlinelibrary.wiley.com/doi/10.1029/2020IA028182, Wiley Online Library on [27/06/2024]. See the Terms and Conditions (https://onlinelibrary.wiley.com/doi/10.1029/2020IA028182, Wiley Online Library on [27/06/2024]. See the Terms and Conditions (https://onlinelibrary.wiley.com/doi/10.1029/2020IA028182, Wiley Online Library on [27/06/2024]. See the Terms and

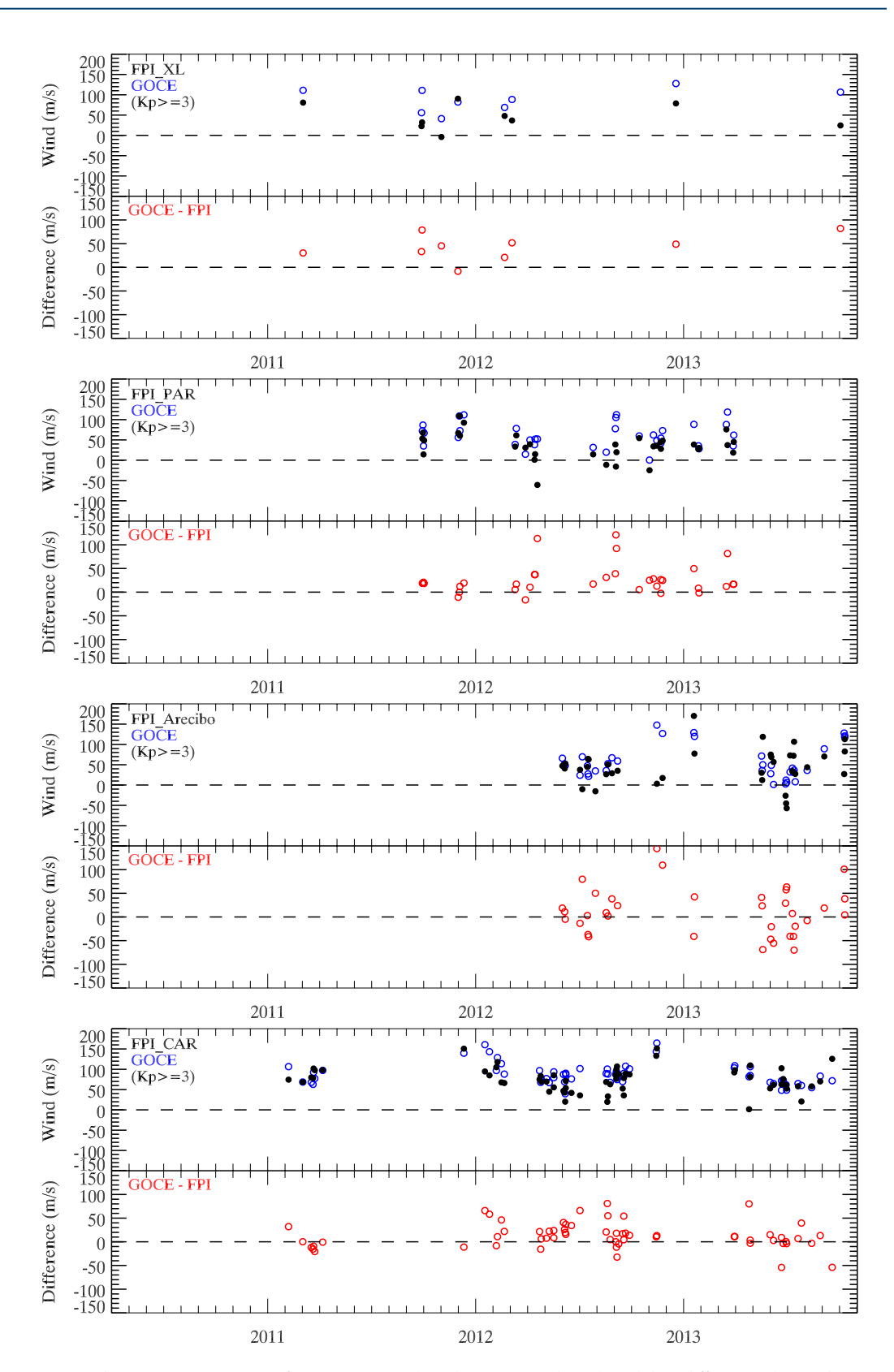


Figure 6. The conjunct time series of GOCE crosswinds and FPI projected winds and their differences during the geomagnetically active days of 2010–2013. FPI, Fabry-Perot interferometers; GOCE, Gravity field and steady-state Ocean Circulation Explorer.

JIANG ET AL. 9 of 16

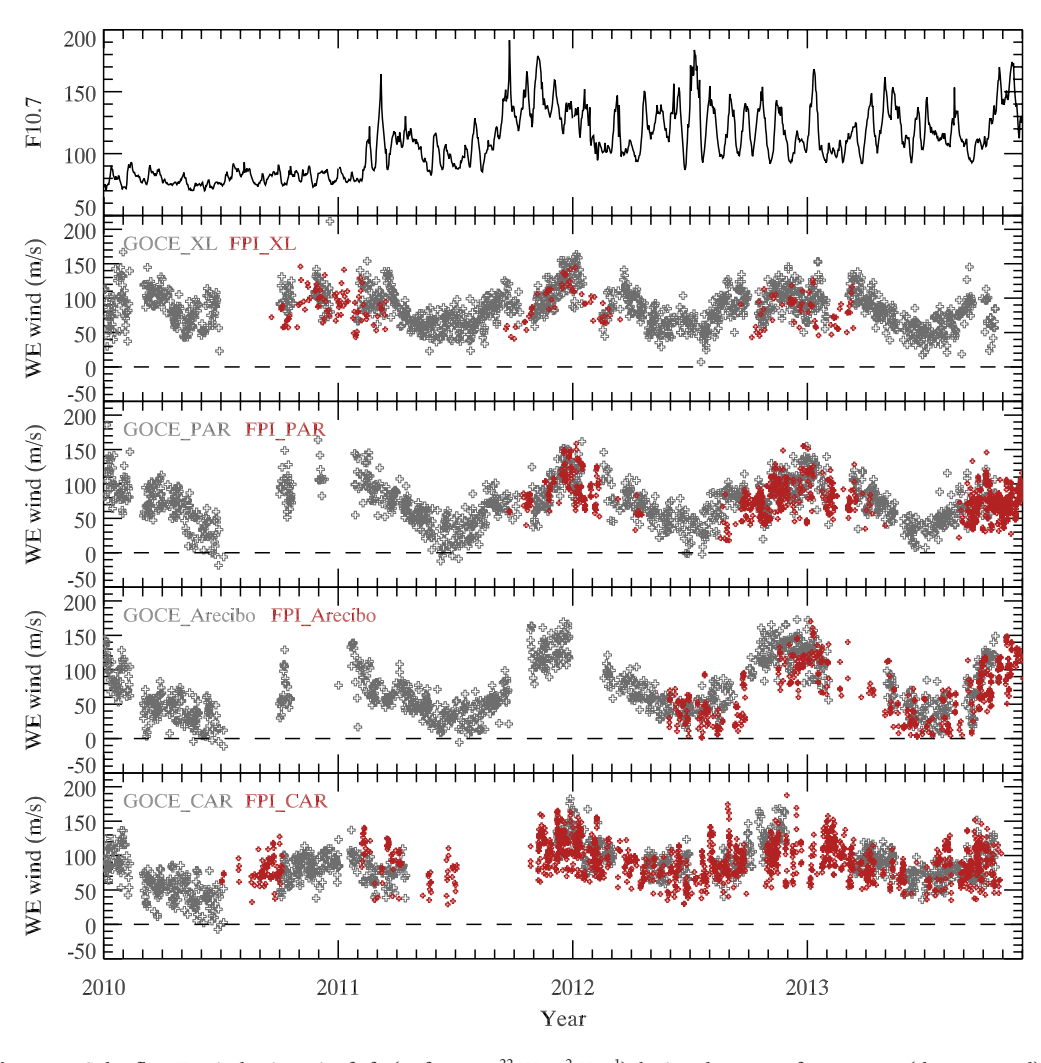


Figure 7. Solar flux $F_{10.7}$ index in unit of sfu (1 sfu = 10^{-22} Wm⁻² Hz⁻¹) during the years of 2010–2013 (the top panel), and the time series of GOCE and FPIs winds on the dusk side during geomagnetically quiet periods over four stations (the second to the fifth panels). Gray cross denotes GOCE measurements; dark red cross denotes FPI observations. FPI, Fabry-Perot interferometers; GOCE, Gravity field and steady-state Ocean Circulation Explorer.

of whether there are conjunction measurements from an FPI or not; while the FPI zonal wind values are depicted as red crosses. A similar annual variation of the dusk side zonal winds, with peak in December and valley in June, is seen from GOCE and all four FPI stations located from middle latitude to around equatorial region. However, slight latitudinal differences are found between the zonal winds at different stations. For example, during the months of June and July the zonal wind over PAR and Arecibo is smaller than that over XL. However, during the months of December and January the FPI zonal wind speeds over these three stations do not show clear differences. The wind variation with seasons shown in Figure 7 is consistent with that shown in Figure 4, which indicates that GOCE crosswind at low and middle latitudes is near to the zonal direction, and the zonal component can represent the variation of the crosswind.

The fifth (bottom) panel illustrates the solar activity dependence of the thermospheric zonal wind over CAR, which is consistent with the result of Liu et al. (2016) that solar flux has a positive effect on the eastward wind in the equatorial region. The zonal wind around equator shows a more significant dependence on solar flux than that at mid-latitudes.

JIANG ET AL. 10 of 16

21699402, 2021, 2, Downloaded from https://agupubs.onlinelibrary.wiley.com/doi/10.1029/2020JA028182, Wiley Online Library on [27/06/2024]. See the Terms and Conditions (https://agupubs.onlinelibrary.wiley.com/doi/10.1029/2020JA028182, Wiley Online Library on [27/06/2024]. See the Terms and Conditions (https://agupubs.onlinelibrary.wiley.com/doi/10.1029/2020JA028182, Wiley Online Library on [27/06/2024]. See the Terms and Conditions (https://agupubs.onlinelibrary.wiley.com/doi/10.1029/2020JA028182, Wiley Online Library on [27/06/2024]. See the Terms and Conditions (https://agupubs.onlinelibrary.wiley.com/doi/10.1029/2020JA028182, Wiley Online Library on [27/06/2024]. See the Terms and Conditions (https://agupubs.com/doi/10.1029/2020JA028182, Wiley Online Library.wiley.com/doi/10.1029/2020JA028182, Wiley Online Library.wiley.wiley.com/doi/10.1029/2020JA028182, Wiley Online Library.wiley.wiley.com/doi/10.1029/2020JA028182, Wiley Online Library.wiley.co

://onlinelibrary.wiley.com/terms-and-conditions) on Wiley Online Library for rules of use; OA articles are governed by the applicable Creative Commons Licensu

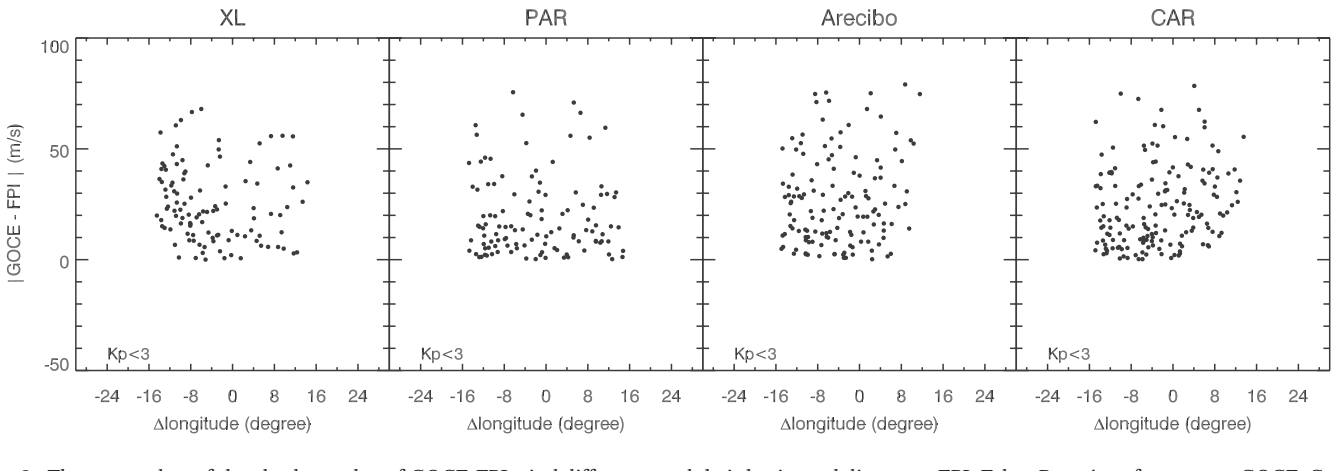


Figure 8. The scatterplots of the absolute value of GOCE-FPI wind difference and their horizontal distances. FPI, Fabry-Perot interferometers; GOCE, Gravity field and steady-state Ocean Circulation Explorer.

4. Discussions

To find the conjunction events between GOCE and ground FPIs, we have considered the events when the longitudinal separation between the two systems is within 15°(corresponding to maximum zonal distance of 1,650 km). Figure 8 presents the variation of wind differences between GOCE and FPI data on their longitudinal separation, however, no clear dependence of the wind differences is found with the longitudinal separation.

To better quantify the relation between GOCE and FPI winds at dusk side, we calculated the average ratio between them separately for geomagnetically quiet and active periods, and the results are listed out in Table 2. As shown by \overline{GOCE} / FPI. The average values between GOCE winds and FPI measurements are quite close for the four stations from middle latitude to around equatorial region: GOCE crosswinds are 1.69 (XL), 1.37 (PAR), 1.44 (Arecibo) and 1.42 (CAR) times larger than FPI measurements during magnetically quiet periods, respectively. During active periods, the averaged ratios are 0.85 (XL), 2.17 (PAR), 2.15 (Arecibo) and 2.15 (CAR), respectively. As shown by the mean value of |GOCE - FPI|, the quiet time absolute wind differences of GOCE and FPI winds are 25.03 m/s, 19.41 m/s, 26.82 m/s and 24.15 m/s at XL, PAR, Arecibo and CAR stations, respectively. It is interesting that the wind differences during active periods are significantly larger than those during quiet periods at XL, PAR and Arecibo, but the comparison at CAR (near equator) has comparable wind differences with 21.82 m/s in active periods and 24.15 m/s in quiet periods, which indicate a relatively smaller effect of geomagnetic activity on the equatorial thermospheric wind.

Kärräng (2015) discussed the relationship of GOCE and ground SDI/FPI winds at high latitude (Poker Flat, geog.: 65.12°N, 147.43°W and Kiruna, geog.: 67.53°N, 21.04°E), which considers the slope of linear fitting between their wind values. Their results showed that the GOCE crosswinds are 1.2–2.0 times stronger than the horizontal wind vector and that their correlation coefficients are 0.60 and 0.89 for Poker Flat SDI and

Table 2
The Averaged Ratio and Difference Between GOCE Crosswinds and FPI Projected Winds at Dusk Side

FPI / STDDEV (m/s)
44.35/24.63
28.44/29.93
40.06/31.90
21.82/20.65

Abbreviations: FPI, Fabry-Perot interferometers; GOCE, Gravity field and steady-state Ocean Circulation Explorer; STDDEV, standard deviation.

JIANG ET AL.

Kiruna FPI, respectively. It is worth noting that the study of Kärräng (2015) did not distinguish between different geomagnetic conditions. M. Dhadly et al. (2017) and M. S. Dhadly et al. (2019) found no major biases among various quiet time data sets of FPIs, SDIs, DE2 WATS and UARS WINDII except for GOCE at high latitude. They found that during quiet time, GOCE high-latitude crosswinds are generally stronger than other data sets on the dusk side, for example, typically \sim 85 m/s larger in average than those of WINDII winds, but there is a better agreement between GOCE and other data sets at dawn side.

We would like to note that the newly released GOCE wind data (version 2.0) are used in our study, but the previous versions of GOCE data were used in the studies of Kärräng (2015), M. Dhadly et al. (2017), and M. S. Dhadly et al. (2019). As pointed out by March et al. (2019b) and T. Visser et al. (2019), instead of tuning the aerodynamic model of GOCE to match the ground-based observations directly, they improved the current accuracy level using high-fidelity geometries and a wide range of the energy accommodation coefficient, which is a key parameter for describing gas-surface interactions. Overall, although different versions of GOCE wind data have been applied in our study and earlier publications, a similar result is derived that the GOCE wind shows larger absolute wind values than the ground-based FPIs. Despite the large absolute value, GOCE wind shows consistent signatures of the wind reversal in the dusk side circulation cell at high latitude (Figure 6 in M. Dhadly et al., 2017) and the seasonal variation of thermospheric wind at middle latitude and around equatorial region (Figures 4, 7, and 9 in this paper) as that observed by ground FPIs.

We finally point out that the discrepancies between the wind data derived from GOCE accelerometer and ground FPIs probably originate in the different measurement techniques. The GOCE technique is measuring an in-situ wind at a specific altitude while the ground-based FPI technique is measuring a height-integrated (and weighted) measurement at a different altitude. GOCE winds are derived from the in-situ records of the accelerometer on board the satellite due to the air drag, whose altitude positioning is much more accurate. The ground-based Fabry-Perot spectrometers (FPI and SDI) estimate the winds based on the measurement of airglow emission (e.g. at 630.0 nm wavelength) layer, whose altitude position covers a wider range with peak volume emission near 240–250 km. Two other possible reasons for the GOCE-FPI discrepancy are: (1) Altitude variations in the winds can exist above 200 km; (2) Atmospheric scattering in the troposphere can cause winds that are several-to-10 percent too low and airglow gradients can be large after sunset, and exacerbate the scattering problem (Harding et al., 2017b).

5. Summary

The newly derived thermospheric winds (version 2.0) from GOCE accelerometer measurements were released in April 2019. In this study, we report the results of statistical comparison between the new GOCE crosswind measurements and the winds from four FPIs located at the Asian and American sector, with latitude ranging from middle latitudes to around equatorial region. Almost all the conjunction measurements of GOCE and FPIs are on the dusk side. The data comparison period is from 2010 to 2013.

Our result shows that during geomagnetically quiet periods the GOCE crosswind on the dusk side presents consistent signatures of annual variations that compare well with those derived from ground-based FPIs, showing largest speed around December and lowest speed around June. However, despite the similarity, the GOCE wind is generally larger than the wind derived from FPIs, with average ratios around 1.37–1.69 for the four stations. The correlation coefficients between data of the four FPIs winds and GOCE winds reach 0.58 for XL, 0.67 for PAR, 0.68 for Arecibo and 0.64 for CAR.

During geomagnetically active periods, the relation between the GOCE and FPI derived winds are generally poorer. The correlation coefficients between GOCE crosswinds and FPI horizontal winds are 0.57 for XL, 0.49 for PAR, 0.32 for Arecibo and 0.54 for CAR, respectively. But still the absolute value of the wind derived from GOCE is larger than that of the FPIs, for the station at Arecibo during June solstice months.

As indicated by the results of the wind comparison in this paper, the discrepancies between the wind data sets from GOCE accelerometer and FPIs should mainly lay in the different measurement principles of the two techniques.

XL FPI is a relatively new instrument. This work provides the first comprehensive validation for the wind measurement by the XL FPI, which was found to provide reliable wind observations in the same quality as

JIANG ET AL. 12 of 16

21699402, 2021, 2, Downloaded from https://agupubs.onlinelibrary.wiley.com/doi/10.10/29/2020IA028182, Wiley Online Library on [27/06/204]. See the Terms and Conditions (https://onlinelibrary.wiley.com/terms-and-conditions) on Wiley Online Library for rules of use; OA articles are governed by the applicable Creative Commons Licensea (Commons Licensea) and Conditions (https://onlinelibrary.wiley.com/terms-and-conditions) on Wiley Online Library for rules of use; OA articles are governed by the applicable Creative Commons Licensea (Commons Licensea) and Conditions (https://onlinelibrary.wiley.com/terms-and-conditions) on Wiley Online Library for rules of use; OA articles are governed by the applicable Creative Commons Licensea (Commons Licensea) and Conditions (https://onlinelibrary.wiley.com/terms-and-conditions) on Wiley Online Library for rules of use; OA articles are governed by the applicable Creative Commons Licensea (Commons Licensea) and Conditions (https://onlinelibrary.wiley.com/terms-and-conditions) on Wiley Online Library for rules of use; OA articles are governed by the applicable Creative Commons Licensea (Commons Licensea) and Conditions (https://onlinelibrary.wiley.com/terms-and-conditions) on Wiley Online Library for rules of use; OA articles are governed by the applicable Creative Commons Licensea (Commons L

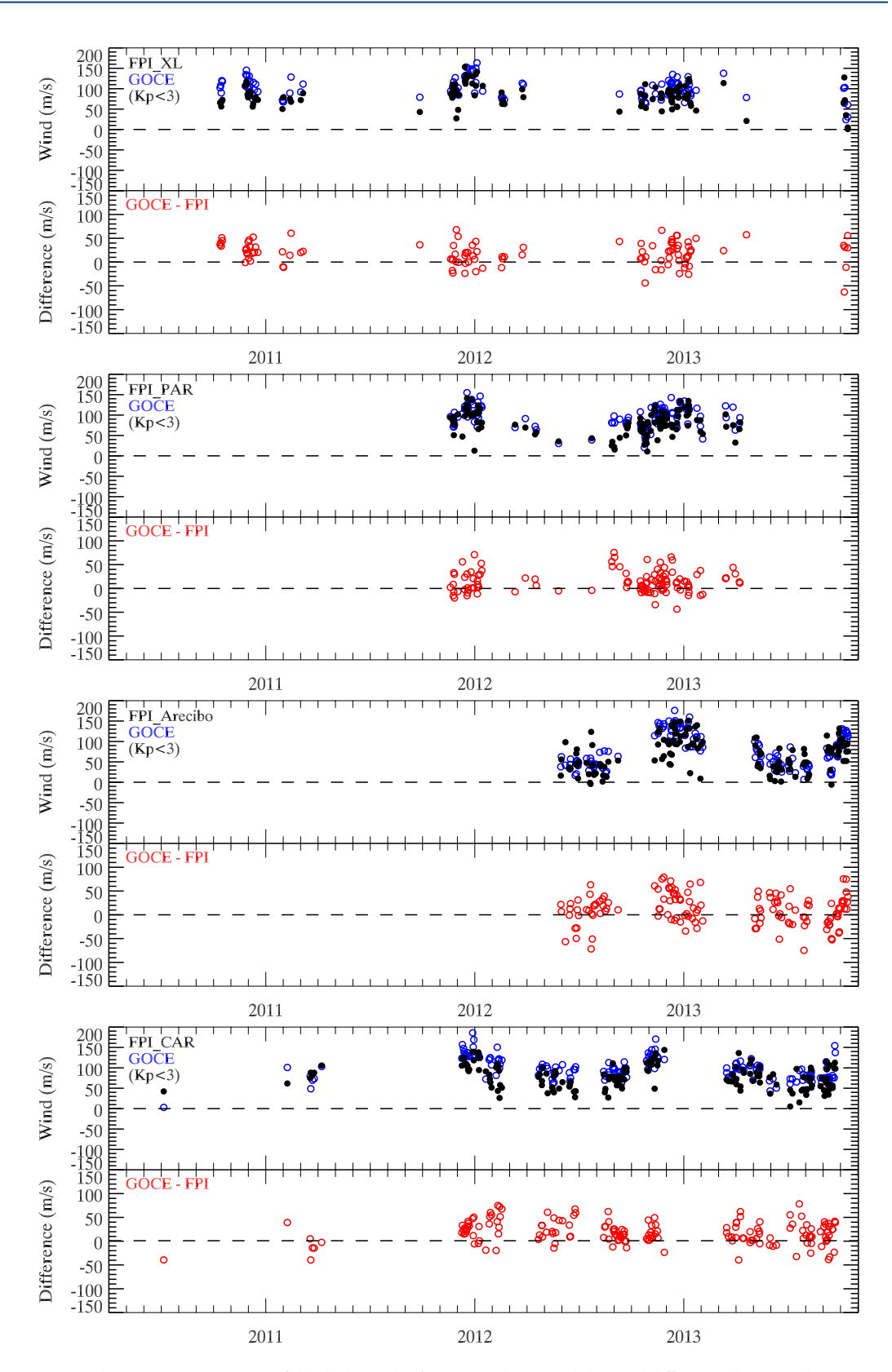


Figure 9. The conjunct time series of the dusk winds of GOCE and FPIs and the wind differences between them during the geomagnetically quiet periods of 2010–2013. FPI, Fabry-Perot interferometers; GOCE, Gravity field and steady-state Ocean Circulation Explorer.

JIANG ET AL. 13 of 16

Journal of Geophysical Research: Space Physics

from established FPIs in the American sector. In future, the XL FPI will provide valuable information for investigating the thermosphere above Asia.

Data Availability Statement

The recalibrated GOCE wind data can be found at https://earth.esa.int/eogateway/missions/goce/goce+-thermospheric-data. The FPI wind data at PAR, Arecibo and CAR stations can be freely downloaded from http://cedar.openmadrigal.org/.

Acknowledgments

The authors want to thank Dr. Eelco Doornbos for fruitful discussions about GOCE data processing. The work of Guoying Jiang is supported by the NNS-FC (grants: 41774159, 41831073) and National Key R&D Program of China (grant: 2018YFC1407305). The work of Chao Xiong is supported by the ESA GOCE-HPF project (Grant 18308/04/ NL/MM). We acknowledge the use of data from the Chinese Meridian Project (http://159.226.22.74/). This work is also supported by the Specialized Research Fund for State Key Laboratories.

References

- Aruliah, A., Förster, M., Hood, R., McWhirter, I., & Doornbos, E. (2019). Comparing high-latitude thermospheric winds from Fabry–Perot interferometer (FPI) and challenging mini-satellite payload (CHAMP) accelerometer measurements. *Ann. Geophys.*, 37, 1095–1120. https://doi.org/10.5194/angeo-37-1095-2019
- Balsley, B. B., Fejer, B. G., & Farley, D. T. (1976). Radar measurements of neutral winds and temperatures in the equatorial E region. *Journal of Geophysical Research*, 81, 1457–1459.
- Biondi, M. A., & Feibelman, W. A. (1968). Twilight and nightglow spectral line shapes of oxygen 6300 and 5577 radiation. *Planetary and Space Science*, 16, 431. https://doi.org/10.1016/0032-0633(68)90158-X
- Burnside, R. G., & Tepley, C. A. (1989). Optical observations of thermospheric neutral winds at Arecibo between 1980 and 1987. *Journal of Geophysical Research*, 94, 2711–2716. https://doi.org/10.1029/JA094iA03p02711
- Dhadly, M. S., Emmert, J. T., Drob, D. P., Conde, M. G., Aruliah, A., Doornbos, E., et al. (2019). HL-TWIM empirical model of high-latitude upper thermospheric winds. *Journal of Geophysical Research: Space Physics*, 124, 10592–10618. https://doi.org/10.1029/2019JA027188
- Dhadly, M. S., Emmert, J. T., Drob, D. P., Conde, M. G., Doornbos, E., Shepherd, G. G., et al. (2018). Seasonal dependence of geomagnetic active-time northern high-latitude upper thermospheric winds. *Journal of Geophysical Research: Space Physics*, 123, 739–754. https://doi.org/10.1002/2017JA024715
- Dhadly, M., Emmert, J., Drob, D., Conde, M., Doornbos, E., Shepherd, G., Makela, J., et al. (2017). Seasonal dependence of northern high-latitude upper thermospheric winds: A quiet time climatological study based on ground-based and space-based measurements. Journal of Geophysical Research: Space Physics, 122, 2619–2644. https://doi.org/10.1002/2016JA023688
- Doornbos, E. (2011). Thermospheric Density and Wind Determination from Satellite Dynamics (PhD. thesis) Delft: Delft Univ. of Technol. Doornbos, E., Bruinsma, S., Fritsche, B., Visser, P., Van Den IJssel, J., Encarnacao, J. T., & Kern, M., (Eds.). (2013). Air density and wind retrieval using GOCE data. ESA Living Planet Symposium, Proceedings of the conference held on 9–13 September 2013 at Edinburgh in United Kingdom, ESA SP-722. 2–13, (p. 7). Netherlands: TU Delft.
- Doornbos, E., van den IJssel, J., Lühr, H., Förster, M., & Koppenwallner, G. (2010). Neutral density and crosswind determination from arbitrarily oriented multi-axis accelerometers on satellites. *Journal of Spacecraft and Rockets*, 47(4), 580–589. https://doi.org/10.2514/1.48114
 Drob, D. P., Emmert, J. T., Meriwether, J. W., Makela, J. J., Doornbos, E., Conde, M., et al. (2015). An update to the Horizontal Wind Model (HWM): The quiet time thermosphere. *Earth and Space Science*, 2, 301–319. https://doi.org/10.1002/2014EA000089
- Emery, B. A. (1978). Neutral thermospheric winds deduced above Millstone Hill: 1. Mathematical model, uncertainties, and representative results. *Journal of Geophysical Research*, 83, 5691–5703.
- Emmert, J. T., Faivre, M. L., Hernandez, G., Jarvis, M. J., Meriwether, J. W., Niciejewski, R. J., et al. (2006). Climatologies of nighttime upper thermospheric winds measured by ground-based Fabry-Perot interferometers during geomagnetically quiet conditions: 1. Local time, latitudinal, seasonal, and solar cycle dependence. *Journal of Geophysical Research*, 111, A12302. https://doi.org/10.1029/2006JA011948
- Emmert, J. T., Fejer, B. G., Fesen, C. G., Shepherd, G. G., & Solheim, B. H. (2001). Climatology of middle- and low latitude F region disturbance neutral winds measured by Wind Imaging Interferometer (WINDII). *Journal of Geophysical Research*, 106, 24701–24712. https://doi.org/10.1029/2000JA000372
- Emmert, J. T., Hernandez, G., Jarvis, M. J., Niciejewski, R. J., Sipler, D. P., & Vennerstrom, S. (2006). Climatologies of nighttime upper thermospheric winds measured by ground-based Fabry-Perot interferometers during geomagnetically quiet conditions: 2. High-latitude circulation and interplanetary magnetic field dependence. *Journal of Geophysical Research*, 111, A12303. https://doi.org/10.1029/2006JA011949
- Fisher, D. J. (2013). Three-dimensional wind measurements and modeling using a bi-static Fabry-Perot interferometer system in Brazil. MS thesis. University of Illinois at Urbana-Champaign.
- Fisher, D. J. (2017). Observations of the thermosphere using measurements from long-term Fabry-Perot interferometers. PhD thesis. University of Illinois at Urbana-Champaign.
- Fisher, D. J., Makela, J. J., Meriwether, J. W., Buriti, R. A., Benkhaldoun, Z., Kaab, M., et al. (2015). Climatologies of nighttime thermospheric winds and temperatures from Fabry-Perot interferometer measurements: From solar minimum to solar maximum. *Journal of Geophysical Research: Space Physics*, 120, 6679–6693. https://doi.org/10.1002/2015JA021170
- Floberghagen, R., Fehringer, M., Lamarre, D., Muzi, D., Frommknecht, B., Steiger, et al. (2011). Mission design, operation and exploitation of the Gravity field and steady-state Ocean Circulation Explorer mission. *Journal of Geodesy*, 85(11), 749–758. https://doi.org/10.1007/s00190-011-0498-3
- Harding, B. J. (2017). Midlatitude thermospheric wind and temperature: Networked fabry-Perot interferometer observations and radiative transfer modeling. PhD thesis, University of Illinois at Urbana-Champaign.
- Harding, B. J., Makela, J. J., Qin, J., Fisher, D. J., Martinis, C. R., Noto, J., et al. (2017). Atmospheric scattering effects on ground-based measurements of thermospheric vertical wind, horizontal wind, and temperature. *Journal of Geophysical Research: Space Physics*, 122, 7654–7669. https://doi.org/10.1002/2017JA023942
- Harding, B. J., Qin, J., & Makela, J. J. (2017). Ground-based optical measurements of quiet time thermospheric wind and temperature: Atmospheric scattering corrections. *Journal of Geophysical Research: Space Physics*, 122, 11624–11632. https://doi.org/10.1002/2017JA024705
 Hedin, A. E., Spencer, N., & Killeen, T. (1988). Empirical global model of upper thermosphere winds based on atmosphere and dynamics
- Hedin, A. E., Spencer, N., & Killeen, T. (1988). Empirical global model of upper thermosphere winds based on atmosphere and dynamics explorer satellite data. *Journal of Geophysical Research: Space Physics*, 93(A9), 9959–9978. https://doi.org/10.1029/JA093iA09p09959

JIANG ET AL. 14 of 16

- Innis, J. L., Greet, P. A., & Dyson, P. L. (1996). Fabry-Perot spectrometer observations of the auroral oval/polar cap boundary above Mawson, Antarctica. Journal of Atmospheric and Terrestrial Physics, 58, 1973–1988.
- Ishii, M., Okano, S., Sagawa, E., Watari, S., Mori, H., Iwamoto, I., et al. (1997). Development of Fabry-Perot interferometers for airglow observations. *Proceedings of the NIPR Symposium on Upper Atmosphere Physics*, 10, 97.
- Jiang, G., Xu, J., Wang, W., Yuan, W., Zhang, S., Yu, T., et al. (2018). A comparison of quiet time thermospheric winds between FPI observations and model calculations. *Journal of Geophysical Research: Space Physics*, 123, 7789–7805. https://doi.org/10.1029/2018JA025424
- Kärräng, P. (2015). Comparison of thermospheric parameters from space- and ground- based instruments (MS thesis). Kiruna, Sweden: Luleå University of Technology.
- Kerr, R. B. (2013). Data from the CEDAR Madrigal database. Computational Physics Inc. Available from https://w3id.org/cedar?experiment_list=experiments/2013/aif/04jan13&file_list=aif130104g00004.hdf5
- Kerr, R. B. (2019). Measurement of thermospheric vertical neutral winds with a single Etalon fabry-Perot interferometer, Abstract SA21B-3099. San Francisco, CA: AGU Fall Meeting.
- Kerr, R. B., Bishop, J., Tepley, C. A., Atreya, S. K., Cageao, R. P., Cherchneff, I. M., et al. (1989). Ground-based measurements of O1D and the H2O production rate from comets. *Advances in Space Research*, 9, 181–190.
- Kerr, R. B., Kapali, S., Riccobono, J., Migliozzi, M. A., Noto, J., Brum, C. G.M., et al. (2017). Climatology of Neutral vertical winds in the midlatitude thermosphere, Abstract SA44A-06. New Orleans, LA: AGU Fall Meeting.
- Killeen, T. L., Hays, P. B., Spencer, N. W., & &Wharton, L. E. (1982). Neutral winds in the polar thermosphere as measured from Dynamics Explorer. *Geophysical Research Letters*, 9(9), 957–960. https://doi.org/10.1029/GL009i009p00957
- King-Hele, D. G. (1964). The rotational speed of the upper atmosphere determined from changes in satellite orbits. Planetary and Space Science, 12, 835–853.
- King-Hele, D. G., & Walker Doreen, M. C. (1983). Upper-atmosphere zonal winds from satellite orbit analysis. *Planetary and Space Science*, 31, 509–535.
- Lei, J., Roble, R. G., Kawamura, S., & Fukao, S. (2007). A simulation study of thermospheric neutral winds over the MU radar. *Journal of Geophysical Research*, 112, A04303. https://doi.org/10.1029/2006JA012038
- Liu, H., Doornbos, E., & Nakashima, J. (2016). Thermospheric wind observed by GOCE: Wind jets and seasonal variations. Journal of Geophysical Research: Space Physics, 121, 6901–6913. https://doi.org/10.1002/2016JA022938
- Liu, H., Lühr, H., Watanabe, S., Köhler, W., Henize, V., & Visser, P. (2006). Zonal winds in the equatorial upper thermosphere: Decomposing the solar flux, geomagnetic activity, and seasonal dependencies. *Journal of Geophysical Research*, 111, A07307. https://doi.org/10.1029/2005JA011415
- Lühr, H., Rentz, S., Ritter, P., Liu, H., & Häusler, K. (2007). Average thermospheric wind patterns over the polar regions, as observed by CHAMP. *Annales Geophysicae*, 25, 1093–1101. https://doi.org/10.5194/angeo-25-1093-2007
- Makela, J. J., Fisher, D. J., Meriwether, J. W., Buriti, R. A., & Medeiros, A. F. (2013). Near-continual ground-based nighttime observations of thermospheric neutral winds and temperatures over equatorial Brazil from 2009 to 2012. *Journal of Atmospheric and Solar-Terrestrial Physics*, 103, 94–102. https://doi.org/10.1016/j.jastp.2012.11.019
- Makela, J. J., Meriwether, J. W., Huang, Y., & Sherwood, P. J. (2011). Simulation and analysis of a multi-order imaging Fabry-Perot interferometer for the study of thermospheric winds and temperatures. *Applied Optics*, 50, 4403–4416.
- Makela, J. J., Meriwether, J. W., Lima, J. P., Miller, E. S., & Armstrong, S. J. (2009). The remote equatorial nighttime observatory of ion-ospheric regions project and the international heliospherical year. Earth, Moon, and Planets, 104, 211–226. https://doi.org/10.1007/s11038-008-9289-0
- Makela, J. J., Meriwether, J. W., Ridley, A. J., Ciocca, M., & Castellez, M. W. (2012). Large-scale measurements of thermospheric dynamics with a multisite Fabry-Perot interferometer network: Overview of plans and results from midlatitude measurements. *International Journal of Geophysics*, 2012(3), 1–10. https://doi.org/10.1155/2012/872140
- March, G., Doornbos, E. N., & Visser, P. N. A. M. (2019). High-fidelity geometry models for improving the consistency of CHAMP, GRACE, GOCE and Swarm thermospheric density data sets. *Advances in Space Research*, 63(1), 213–238. https://doi.org/10.1016/j.asr.2018.07.009
- March, G., Visser, T., Visser, P. N. A. M., & Doornbos, E. N. (2019). CHAMP and GOCE thermospheric wind characterization with improved gas-surface interactions modelling. *Advances in Space Research*, 64(6), 1225–1242. https://doi.org/10.1016/j.asr.2019.06.023
- Marcos, F. A., & Forbes, J. M. (1985). Thermospheric winds from the satellite electrostatic triaxial accelerometer system. *Journal of Geophysical Research*, 90, 6543–6552.
- Meriwether, J. W. (2006). Studies of thermospheric dynamics with a Fabry-Perot interferometer network: A review. *Journal of Atmospheric and Solar-Terrestrial Physics*, 68, 1576–1589.
- Noto, J., Kerr, R. B., Ng, K., Lancaster, R. S., & Dorin, M. (1994). Boston University's high-resolution near-infrared Fabry-Perot spectrometer. *Optical Engineering*, 33(2), 451–456.
- Rees, D., Fuller-Rowell, T., & Smith, R. W. (1980). Measurements of high latitude thermospheric winds by rocket and ground-based techniques and their interpretation using a three-dimensional time-dependent dynamical model. *Planetary and Space Science*, 28, 919–932.
- Richmond, A. D., Ridley, E. C., & Roble, R. G. (1992). A thermosphere/ionosphere general circulation model with coupled electrodynamics. *Geophysical Research Letters*, 19, 601–604. https://doi.org/10.1029/92GL00401
- Shepherd, G. G., Thuillier, G., Gault, W. A., Solheim, B. H., Hersom, C., Alunni, J. M., et al. (1993). WINDII, the Wind Imaging Interferometer on the Upper Atmosphere Research Satellite. *Journal of Geophysical Research*, 98, 10725–10750. https://doi.org/10.1029/93JD00227
- Spencer, N. W., Wharton, L. E., Niemann, H. B., Hedin, A. E., Carignan, G. R., & Maurer, J. C. (1981). The Dynamics Explorer wind and temperature spectrometer. *Space Science Instrumentation*, 5, 417–428.
- Sutton, E. K. (2008). Effects of solar disturbances on the thermosphere densities and winds from CHAMP and GRACE satellite accelerometer data, (Doctoral Dissertation). Boulder, Colorado: Department of Aerospace Engineering Sciences, University of Colorado.
- Visser, T., Doornbos, E., de Visser, C., Visser, P., & Fritsche, B. (2018). Torque model verification for the GOCE satellite. *Advances in Space Research*, 62(5), 1114–1136. https://doi.org/10.1016/j.asr.2018.06.025
- Visser, T., March, G., Doornbos, E., de Visser, C., & Visser, P. (2019). Horizontal and vertical thermospheric cross-wind from GOCE linear and angular accelerations. *Advances in Space Research*, 63(10), 3139–3153. https://doi.org/10.1016/j.asr.2019.01.030
- Visser, P., & van den IJssel, J. (2016). Calibration and validation of individual GOCE accelerometers by precise orbit determination. *Journal of Geodesy*, 90, 1–13. https://doi.org/10.1007/s00190-015-0850-0
- Wang, C. (2010). New Chains of Space Weather Monitoring Stations in China. Space Weather, 8, S08001. https://doi.org/10.1029/2010SW000603
- Wu, Q., Gablehouse, R. D., Solomon, S. C., Killeen, T. L., & She, C. Y. (2004). A new Fabry-Perot interferometer for upper atmospheric research. Proceedings of SPIE-The International Society for Optical Engineering, 5660, 218–277.

JIANG ET AL. 15 of 16



Journal of Geophysical Research: Space Physics

10.1029/2020JA028182

- Wu, Q., Ortland, D. A., Killeen, T. L., Roble, R. G., Hagan, M. E., Liu, H.-L., et al. (2008). Global distribution and interannual variations of mesospheric and lower thermospheric neutral wind diurnal tide: 1. Migrating tide. *Journal of Geophysical Research*, 113, A05308. https://doi.org/10.1029/2007JA012542
- Xiong, C., Lühr, H., & Fejer, B. G. (2015). Global features of the disturbance winds during storm time deduced from CHAMP observations. Journal of Geophysical Research: Space Physics, 120, 5137–5150. https://doi.org/10.1002/2015JA021302
- Yuan, W., Liu, X., Xu, J., Zhou, Q., Jiang, G., & Ma, R. (2013). FPI observations of nighttime mesospheric and thermospheric winds in China and their comparisons with HWM07. *Annales Geophysicae*, 31, 1365–1378. https://doi.org/10.5194/angeo-31-1365-2013
- Yuan, W., Xu, J., Ma, R., Wu, Q., Jiang, G., Gao, H., et al. (2010). First observation of mesospheric and thermospheric winds by a Fabry-Perot interferometer in China. *Chinese Science Bulletin*, 55, 4046–4051. https://doi.org/10.1007/s11434-010-4192-2
- Yu, T., Huang, C., Zhao, G., Mao, T., Wang, Y., Zeng, Z., et al. (2014). A preliminary study of thermosphere and mesosphere wind observed by Fabry-Perot over Kelan, China. *Journal of Geophysical Research: Space Physics*, 119, 4981–4997. https://doi.org/10.1002/2013JA019492
- Zhang, X., Liu, L., & Liu, S. (2017). Dependence of thermospheric zonal winds on solar flux, geomagnetic activity, and hemisphere as measured by CHAMP. *Journal of Geophysical Research: Space Physics*, 122, 8893–8914. https://doi.org/10.1002/2016JA023715

JIANG ET AL. 16 of 16